# PARKINSON'S DISEASE-ASSOCIATED PINK1 LOSS DISRUPTS VESICLE TRAFFICKING IN ENSHEATHING GLIA CAUSING DOPAMINERGIC NEURON SYNAPSE LOSS

Lorenzo Ghezzi[1,2], Ulrike Pech[1,2], Nils Schoovaerts[1,2], Suresh Poovathingal[1,2,3], Kristofer Davie[1,2,], Jochen Lamote[1,3], Roman Praschberger[1,2,4,#], Patrik Verstreken[1,2,#]

[1]VIB-KU Leuven Center for Brain & Disease Research; Leuven, Belgium.

[2]KU Leuven, Department of Neurosciences, Leuven Brain Institute, Leuven, Belgium.

[3] VIB Flow Core Leuven, VIB Technologies, Leuven, Belgium

[4]Medical University of Innsbruck, Institute of Human Genetics; Innsbruck, Austria.

[#]Correspondence: patrik.verstreken@kuleuven.be, roman.praschberger@i-med.ac.at

## ABSTRACT

Parkinson's disease (PD) is commonly associated with the loss of dopaminergic neurons in the *substantia nigra*, but many other cell types are affected even before neuron loss occurs. Recent studies have linked oligodendrocytes to early stages of PD, though their precise role is still unclear. *Pink1* is mutated in familial PD and through unbiased single-cell sequencing of the entire brain of *Drosophila Pink1* models, we observed significant gene deregulation in ensheathing glia (EG); cells that share functional similarities with oligodendrocytes. We found that the loss of *Pink1* leads to the activation of EG, similar to the reactive response of EG seen upon nerve injury. Using cell-type specific transcriptomics, we identified deregulated genes in EG as potential functional modifiers. Specifically, downregulating two trafficking factors, Rab7 and Vps13, also mutated in PD, or the direct regulators of Rab7, Mon1 and Ccz1, specifically in EG was sufficient to rescue neuronal function and protect against dopaminergic synapse loss. Our findings demonstrate that Pink1 loss in neurons triggers an injury response in EG, and that Pink1 loss in EG in turn disrupts neuronal function. Vesicle trafficking components, which regulate membrane interactions between organelles within EG, play a crucial role in maintaining neuronal health and preventing dopaminergic synapse loss. Our work highlights the essential role of glial support cells in the pathogenesis of PD and identifies vesicle trafficking within these cells as a key point of convergence in disease progression.

## INTRODUCTION

Parkinson's disease (PD) is characterized by motor symptoms such as bradykinesia, rigidity and tremor that are caused by the progressive loss of dopaminergic neurons in the substantia nigra (Lang & Lozano, 1998). However, most of the patients report non-motor symptoms such as constipation, hyposmia and sleep defects even before the onset of motor symptoms (Munhoz et al., 2015). This suggests that PD is a progressive neurodegenerative disease that initiates many years before the diagnosis and involves different neuronal systems, multiple anatomical areas and different cell types. While therapies symptomatically improve motor functioning temporarily by restoring dopaminergic tone, they do not effectively prevent neurodegeneration and disease progression. This highlights the necessity to identify cell-types and biological mechanisms that act at the earliest stages of disease.

With the advent of single-cell sequencing applied to PD and control brains in combination with evidence from genome-wide association studies (GWAS), it is now possible to suggest which cells and mechanisms are at play at early stages of PD. Among these, a recent study reported that genes related to GWAS loci are highly enriched for oligodendrocyte-specific gene expression (Bryois et al., 2020). Interestingly, differential gene expression in post-mortem brains with Braak scores of 1-2, 3-4, and 5-6 and controls, suggested a role for oligodendrocytes at an early stage of PD prior to the overt loss of dopaminergic neurons(Bryois et al., 2020). Additionally, two independent single-cell sequencing studies, one of the human substantia nigra and one of the midbrain, both associated PD genetic risk with oligodendrocyte-specific expression patterns (Agarwal et al., 2020; Smajic et al., 2022). While these studies started to link dysfunction of oligodendrocyte-cells to the early stages of PD, they did not address their role in the pathophysiology of the disease.

Here we describe a new *Drosophila* model to assess how this neuron-glia cross-talk contributes to PD. *Drosophila* has been successfully used to investigate cellular and molecular dysfunction preceding the onset of age-related symptoms, including dopaminergic neuron-dependent motor symptoms (Kaempf et al., 2024; Pech et al., 2024; Valadas et al., 2018). *Drosophila* glial cells also display several anatomical and functional features that show remarkable similarity to their mammalian counterparts (Freeman & Doherty, 2006; Kremer et al., 2017). While the small size of the *Drosophila* brain does not necessitate elaborate myelination, ensheathing glia (EG) in this species share not only anatomical features with oligodendrocytes, such as the ability to wrap around nerve tracts in the CNS (Kremer et al., 2017; Yildirim et al., 2019), but also important molecular and functional features, such as providing metabolic support and regulating neuronal activity (Delgado et al., 2018; Otto et al., 2018).

In a brain-wide single-cell sequencing experiment, we identified EG as the most deregulated cell type in young (pre-motor) *Pink1* loss-of-function *Drosophila* model. Using cell-specific labeling, immunohistochemistry and electrophysiological recordings, we correlated the transcriptional deregulation in EG with an "active cell state" also seen upon nerve injury, and showed that healthy EG are fundamental to support dopaminergic synapse integrity in *Pink1* mutants. Finally, using cell-type-specific transcriptomic and a high-throughput screening and immunohistochemistry, we identified *Rab7* and *Vps13* as EG-expressed modifiers that maintain dopaminergic synapse-integrity. Our study shows that neuron-ensheating glia crosstalk is disrupted already at young age by the loss of *Pink1* in neurons but also in EG and that EG are fundamental to support dopaminergic synapse-integrity, suggesting a role for oligodendrocytes in the progression of PD.

## RESULTS

### *Ensheating glia in Pink1 loss of function flies are activated non-cell autonomously*

We previously created a whole-brain single-cell RNAseq dataset from different *Drosophila* PD knock-in models. This dataset was generated from young 5-day-old flies to capture 'early' changes (Pech et al, 2024). We re-analyzed the data from *Pink1*$^{P399L}$ knock-in loss-of-function mutant flies and isogenetic controls, and performed differential gene expression (DEG) analysis for each cell type using DESeq2 (Figure 1A). Glial cell subtypes show the highest degree of deregulation; particularly ensheathing glia are strongly affected (Figure 1A). While flies do not myelinate neurons, ensheating glia (EG) serve similar supporting functions to oligodendrocytes (Otto et al., 2018; Yildirim et al., 2019). These results suggest that ensheating glia are deregulated in young *Pink1*$^{P399L}$ mutants (and also *Pink1*$^{KO}$, see below) at an age prior to dopaminergic neuron-dependent motor defects (Kaempf et al., 2024; Pech et al., 2024).

When neurons are damaged, activated EG invade the neuropil (Doherty et al., 2009; MacDonald et al., 2006). For example, when fly antennal lobes are removed, severing the olfactory Olfactory Receptor Neurons (ORNs), EG invade the antennal lobe neuropil (MacDonald et al., 2006), potentially as a protective response (Figure 1B'-C). We tested if EG invade the neuropil in *Pink1* mutant flies and expressed a transmembrane fluorescent protein (*UAS-CD8GFP*) under the control of a promoter specific to EG (*MZ709-Gal4*) in control and *Pink1*$^{KO}$ flies. Samples were labeled with anti-GFP and the pre-synaptic protein Bruchpilot (NC82). Similar to ORN-severed controls, EG invade the antennal neuropil in *Pink1*$^{KO}$, and severing the ORN in *Pink1*$^{KO}$ does not further exacerbate this phenotype (Figure 1B"-C). These data suggest that *Pink1* loss triggers EG activation, similar to neuron-severing, to invade the ORN neuropil.

In order to determine whether this activation is cell-autonomous, we generated cell-type specific *Pink1* perturbations. We either downregulated *Pink1* using a previously well-validated RNAi line specifically in EG (EG-specific *Pink1* loss-of-function – Figure 1D'), or we re-expressed wild-type *Pink1* specifically in EG in *Pink1*$^{KO}$ flies (all cells, but the EG, loss-of-function - Figure 1D"). When *Pink1* is knocked-down in EG (but present in other cells, including neurons), EG do not invade the neuropil (Figure 1D'-1E). However, when *Pink1* is not present in neurons and expressed in EG, the EG do invade the antennal neuropil (Figure 1D"-E). This suggests that *Pink1*-defective neurons activate the EG in a cell-non autonomous fashion to invade, and potentially protect, the neuropil.

***Ensheathing glia function supports synaptic integrity***

Our finding that *Pink1*$^{KO}$ in neurons elicits an EG activation response, suggested that EG might in turn also functionally modulate neuronal integrity in mutant flies. To test this we made use of a readily accessible model circuit in the fly visual system with an easy electrophysiological read-out, Electroretinograms (ERG). The ERG waveforms are susceptible to changes in intracellular signaling, neuronal function and synaptic transmission and have been well characterized, and amply used to assess neuronal and cellular function(Hardie & Raghu, 2001; Praschberger et al., 2023; Soukup et al., 2016; C. F. Wu & Wong, 1977). We exploited this method to understand the role of *Pink1* in EG on neuronal function and synaptic transmission in young flies.

Comparing control with young *Pink1*$^{KO}$ flies does not show a difference in the "depolarization-response", indicating that -as expected- there is no neurodegeneration occurring in the photoreceptors at this stage (Figure 2A). However, when comparing the ON peak – which represents synaptic transmission from the photoreceptors and within the underlying neuronal circuit – we detect a significant reduction in the mutant flies compared to the control, suggesting that in *Pink1*$^{KO}$ flies synaptic communication in this circuit is partially impaired, already at 5 days old (Figure 2A-B).

In order to discern the role of EG in this defective ERG response, we (1) downregulated *Pink1* specifically in EG and (2) we expressed *Pink1* specifically in EG of *Pink1*$^{KO}$. When *Pink1* is knocked down specifically in EG, we observe the same reduction in ON peak response as in the *Pink1*$^{KO}$ flies. This indicates that EG integrity is necessary for efficient neurotransmission in this circuit. Conversely, the ON peak defect of *Pink1*$^{KO}$ mutants is rescued when *Pink1* is reintroduced in EG only. This suggests that activated EG are able to at least partially buffer the detrimental effects of *Pink1* deficiency in neurons (Figure 2A-B).

To also test EG function in relation to PD-relevant dopaminergic (DA) synapses we evaluated the loss of dopaminergic neuron afferents. We previously showed that the loss of *Pink1* function causes a progressive loss of protocerebral anterior medial dopaminergic neuron (PAM DAN) afferents in the

Mushroom Body neuropil (Kaempf et al., 2024) and confirm here that 5 days old *Pink1*$^{KO}$ flies do not show a decrease in the dopaminergic synaptic area in the mushroom bodies (MB) lobes, while aged, 25 days old animals, do (Figure 2 C-D). Hence, while ensheathing glia are already activated at young age in *Pink1*$^{KO}$, DA synapses are structurally still intact and only deteriorate in older flies. We then knocked down *Pink1* specifically in EG and find a similar strong decrease in DA synaptic area (Figure 2C'-D). Conversely, when *Pink1* is reintroduced specifically in EG of *Pink1*$^{KO}$ animals, DA synapse-loss is significantly rescued (Figure 2C"-D). Together, these results indicate that *Pink1* in EG is necessary to protect dopaminergic neurons from synapse loss.

***EG cell type-specific transcriptomics reveals modifiers of neuronal dysfunction***

To identify pathways in EG that are deregulated by *Pink1*$^{KO}$ loss-of-function, we optimized a method to isolate EGs specifically from the rest of the brain, enabling us to perform much higher-sensitivity transcriptomics than what we achieved with our 10x droplet-based single-cell sequencing (Pech et al., 2024). We expressed a fluorescently-tagged histone (UAS-HisTag-eGFP) in EG (GMR-56-gal4) and used Fluorescence-activated Cell Sorting (FACS) to isolate EG. We sorted 300 cells per technical replicate, and performed Bulk-RNA sequencing using a SMART-seq2 protocol (Figure 3A). The sequencing results of EG-sorted cells and of neuron-sorted cells (nsyb-Gal4 instead of GMR-56-gal4) show strong enrichment of EG cell markers in the former and strong enrichment of neuronal markers in the latter (Figure 3B). We then compared the transcriptomic profile of EG in *Pink1*$^{KO}$ to control using differential expression analysis and find 617 deregulated genes in EG (Appendix 1, padj<0.05). To understand whether the deregulated genes were enriched for a specific pathway or associated with a cellular component compared to non-significantly deregulated genes, we performed GO analysis of the deregulated genes in *Pink1*$^{KO}$ flies. Our analysis resulted in generic terms and very diverse pathways that did not allow us to draw further conclusions.

To test if the genes deregulated in EG are modifiers of the neuronal *pink1*$^{KO}$ phenotypes, we downregulated and upregulated (when possible) the 50 most deregulated genes, for which we could find RNAi fly lines, specifically in the EG of *Pink1*$^{KO}$ and recorded ERGs in 5 days old flies. Several of the genes show a rescue of the ON transient defects in *Pink1*$^{KO}$ (4 were significant suppressors at p<0.05) and few exacerbate the defect (Figure 3D). Among the 4 significant suppressors of the *Pink1*$^{KO}$ phenotypes, 3 (*Ccz1*, *CG10646, CG17660*) are associated with endosomal membranes - or their human ortholog is - (Figure 3C-D) (Borchers et al., 2023; Epp et al., 2011; Gaudet et al., 2011; Gershlick et al., 2016). Hence, several DEG in EG of *Pink1*$^{KO}$ are modifiers of the *Pink1* ERG mutant phenotype, and most of those are associated with the endosome.

***Rab7 and Vps13 downregulation in EG rescue synaptic dopaminergic neurons afferent loss***

Among the genes associated with the endosome that we identified in our ERG screening, the strongest suppressors, *Ccz1*, is associated with late endosome function. In particular, Ccz1 forms together with Mon1 a guanosine-nucleotide-exchange factor (GEF) that recruits Rab7 to the endosome (Borchers et al., 2023; Epp et al., 2011). Interestingly, Rab7 is known to physically interact with a peripheral membrane protein that is also causative of PD, Vps13 (Vonk et al., 2017). We therefore also tested if *Rab7*, *Mon1*, and *Vps13* are also *Pink1*-modifiers and find that the knockdown of each of these genes also rescues the ON transient defect of *Pink1*$^{KO}$ mutants (Figure 4A'-B).

To determine if manipulation of vesicle trafficking specifically in EG can rescue PAM DAN synaptic innervation in old (20-25 day old) *Pink1*$^{KO}$ mutants, we expressed RNAi to *Ccz1, Vps13, Rab7* or *Mon1* using mz709-Gal4. Anti-TH labeling (marking DAN synapses) in the Mushroom Body area (marked by anti-DLG) is significantly reduced in *Pink1*$^{KO}$, but rescued to control levels when any of the four genes are knocked down (Figure 4D). These results indicate that Rab7-mediated membrane trafficking in EG regulate glia-neuron crosstalk to maintain synaptic integrity of dopaminergic neuron synapses in the fly brain of *Pink1* mutants.

**DISCUSSION**

In this work, we show there is early, non-cell-autonomous activation of EG in a PD-relevant *Drosophila Pink1* model. This occurs already in young *Pink1*-mutant flies when neuronal defects in dopaminergic neurons are not yet measurable. The EG activation and invasion phenotype appears as a protective response, as *Pink1*-deficient neurons seem to drive EG activation in a manner that mimics the response to nerve injury (Doherty et al., 2009; MacDonald et al., 2006). In addition to EG activation, we show there is also a non-autonomous role of EG to support *Pink1*-deficient neurons. When we manipulate the expression of membrane-lipid trafficking genes, including the homolog of the established PD gene VPS13C (Lesage et al., 2016), specifically in EG, we rescue the dysfunction of *Pink1* mutant neurons. Our work shows the importance of neuron-glia cross-talk in the context of *Pink1*-deficiency. We find (1) there is early EG activation secondary to *Pink1*-loss-induced neuronal impairments; (2) there are specific lipid- and membrane trafficking problems caused by *Pink1* loss in EG that center on Rab7-signaling and (3) there is a convergence of Parkinson-relevant genetic factors that act in EG to maintain neuronal function.

The loss of Pink1 function in the context of Parkinson's disease has been amply linked to the regulation of mitochondrial health. Pink1 maintains the integrity of the electron transport chain by phosphorylating NDUFA10 (Morais et al., 2009, 2014; Pogson et al., 2014) and when mitochondria are damaged, it phosphorylates Parkin and Ubiquitin to facilitate mitophagy (Kane et al., 2014;

Narendra et al., 2010; Narendra & Youle, 2024). The regulation of mitophagy is complex and requires mitochondrial rearrangements controlled by mitochondria-organelle contacts (ER and lysosomes) (Wong et al., 2018, 2019; Yamano et al., 2018). Such contacts mediate inter-organellar lipid exchange as well as facilitate organellar fusion (Kumar et al., 2018; Valadas et al., 2018). In *Pink1* mutants these contacts are increased in number and this causes cellular defects (Grossmann et al., 2023; Valadas et al., 2018).

We found that in EG, *Rab7* and genes encoding proteins that regulate the Rab7 GTPase, functionally interact with Pink1-induced neuronal dysfunction: their genetic manipulation in EG rescues cell non-autonomous neuronal dysfunction. Loss of *Rab7* itself, or loss of *Mon1* and *Ccz1*, only in EG are sufficient to rescue neuronal *Pink1* phenotypes. Mon1 and Ccz1 form a guanine exchange factor (GEF) that specifically loads Rab7 with GTP, thereby activating the protein (Borchers et al., 2023). This is interesting because Rab7-GTP promotes the formation of mitochondria-organelle contacts (mitochondria-lysosome contacts) (Wong et al., 2018). This is also further supported by previous observations showing that overexpression of Fis1 rescues *Pink1* mutant phenotypes: Fis1 localizes to mitochondria to recruit TBC1D15 (Wong et al., 2018), a Rab7 GTPase Activating Protein that hydrolyzes GTP bound to Rab7, thereby inactivating the protein and promoting untethering of lysosome-mitochondrial contacts (Wong et al., 2018). Hence, conditions that inhibit Rab7-GTP-mediated mitochondria-organelle contacts (eg by inhibiting Rab7-GEF or activating Rab7-GAP) in EG rescue *Pink1* neuronal dysfunction, possibly by negatively regulating the stability of organelle contacts in *Pink1* mutants.

Our observation that downregulation of *Vps13* in EG also rescues *Pink1* is in further support of a role for organelle membrane contact site regulation. Vps13 physically interacts with Rab7 (Vonk et al., 2017) and it has two mammalian homologs, VPS13A and VPS13C (Vonk et al., 2017; Vrijsen et al., 2022), that is also mutated in familial PD (Lesage et al., 2016). VPS13A tethers ER to mitochondria and lipid droplets and VPS13C tethers ER to late endosomes, lysosomes and lipid droplets (Kumar et al., 2018; Muñoz-Braceras et al., 2019; Vrijsen et al., 2022). The function of these proteins is to facilitate lipid transfer between organelles, a function we previously showed to be increased in *Pink1* mutants (Valadas et al., 2018). Hence, the downregulation of *Vps13*, similar to *Rab7* or its regulators, would counteract the effects of excessive organelle membrane contact formation and dysregulated lipid homeostasis in *Pink1* mutants.

Lipid homeostasis in glial cells is crucial for supporting neuronal function by providing energy, protecting against oxidative stress, and regulating synaptic health. In oligodendrocytes, maintaining myelin sheaths is critical (Ettle et al., 2016; Lappe-Siefke et al., 2003). While fly EG do not generate

such structures, they do wrap processes around neuropil regions, also requiring lipid membrane production (Kremer et al., 2017; Pogodalla et al., 2021). Through lipid metabolism, glia also supply neurons with essential metabolites, cholesterol, and signaling molecules that aid in membrane integrity, synaptic remodeling, and neuroprotection (Delgado et al., 2018; Otto et al., 2018; Saab et al., 2016; Suárez-Pozos et al., 2020). Further work is now required to define which functions supported by organelle contact sites in glial cells drive cell-nonautonomous protective mechanisms in neurons. Our work in flies indicates these glial defects precede dopaminergic synapse loss, and, importantly, that rescuing the glial defects rescues the dopaminergic problems later in life, underscoring the significance for therapeutic development.

## METHODS

### Resource availability

*Lead Contact*

Further information and requests for resources and reagents should be directed to the lead

contact, Patrik Verstreken (patrik.verstreken@kuleuven.be).

*Materials Availability*

Data, code, Drosophila models, and reagents are available upon request.

### Fly stocks

The fruit flies were maintained in an incubator at 25°C under a 12:12 light-dark cycle, and provided with a standard diet consisting of cornmeal and molasses. For experiments, only fly males were used. Flies were raised in parallel on the same batch of food, which was exchanged every three to four days and kept in only male population of similar density. Flies were aged to 5 ± 1 days old, and 22 ± 2 days old as indicated for immunohistochemistry and ERGs respectively.

To create a set of *Drosophila* models for Parkinson's disease, CRISPR/Cas9-based gene editing was utilized, as outlined in (Kaempf et al., 2024; Pech et al., 2024). In brief, each knockout line contained an attP-flanked w+ reporter cassette that replaced the first shared exon across different isoforms of the targeted gene. For this study, we used knockout flies for *Pink1* from this collection (Kaempf et al., 2024). The "control" strain denotes a semi-isogenized w1118 strain that underwent backcrossing to Canton-S for 10 successive generations, resulting in a strain termed Canton-S-w1118. To generate the fly line Yw; ; UAS-His2Av::eGFP.VK27/TM3Sb, we created the pUASTattB_His2AV-GFP plasmid, linearizing the pUAST.attB (Bischof et al., 2007) with EcoRI-BamHI. A gBlock, containing the His2AV, GS linker and eGFP sequence, was cloned into this linearized plasmid with Gibson Assembly. The

plasmid was inserted into the VK27 landing site by BestGene. The sequence His2AV-GS-eGFP gblock is:TGAATAGGGAATTGGGcAAacATGGCTGGCGGTAAAGCAGGCAAGGATTCGGGCAAGGCCAAGGCGAAGG CGGTATCGCGTTCCGCGCGCGCGGGTCTTCAGTTCCCCGTGGGTCGCATCCATCGTCATCTCAAGAGCCGCACT ACGTCACATGGACGCGTCGGAGCCACTGCAGCCGTGTACTCCGCTGCCATATTGGAATACCTGACCGCCGAGG TCCTGGAGTTGGCAGGCAACGCATCGAAGGACTTGAAAGTGAAACGTATCACTCCTCGCCACTTACAGCTCGC CATTCGCGGAGACGAGGAGCTGGACAGCCTGATCAAGGCAACCATCGCTGGTGGCGGTGTCATTCCGCACAT ACACAAGTCGCTGATCGGCAAAAAGGAGGAAACGGTGCAGGAcCCGCAGCGGAAGGGCAACGTCATTCTGTC GCAGGCCTACGGTTCAGGCGGAGGTGGCAGCGGCGGTGGCGGATCCATGGTGAGCAAGGGCGAGGAGCTG TTCACCGGGGTGGTGCCCATCCTGGTCGAGCTGGACGGCGACGTAAACGGCCACAAGTTCAGCGTGTCCGGC GAGGGCGAGGGCGATGCCACCTACGGCAAGCTGACCCTGAAGTTCATCTGCACCACCGGCAAGCTGCCCGTG CCCTGGCCCACCCTCGTGACCACCCTGACCTACGGCGTGCAGTGCTTCAGCCGCTACCCCGACCACATGAAGCA GCACGACTTCTTCAAGTCCGCCATGCCCGAAGGCTACGTCCAGGAGCGCACCATCTTCTTCAAGGACGACGGC AACTACAAGACCCGCGCCGAGGTGAAGTTCGAGGGCGACACCCTGGTGAACCGCATCGAGCTGAAGGGCATC GACTTCAAGGAGGACGGCAACATCCTGGGGCACAAGCTGGAGTACAACTACAACAGCCACAACGTCTATATCA TGGCCGACAAGCAGAAGAACGGCATCAAGGTGAACTTCAAGATCCGCCACAACATCGAGGACGGCAGCGTGC AGCTCGCCGACCACTACCAGCAGAACACCCCCATCGGCGACGGCCCCGTGCTGCTGCCCGACAACCACTACCT GAGCACCCAGTCCGCCCTGAGCAAAGACCCCAACGAGAAGCGCGATCACATGGTCCTGCTGGAGTTCGTGACC GCCGCCGGGATCACTCTCGGCATGGACGAGCTGTACAAATAAGGGTACCTCTAGAGGATCTT.

Flies were backcrossed for five generations into an inbred Canton-S strain harboring the w1118 mutations. The following genotypes were used in this study:

| Genotype | Abbreviation | Identifier |
|---|---|---|
| w[1118] | W1118 | Kaempf et al., 2024 |
| w[1118] TI{w[+]=white-STAR}Pink1[KOWS]/FM7a | Pink1$^{KO-WS}$ | Kaempf et al., 2024 |
| Yw; ; UAS-His2Av::eGFP.VK27/TM3Sb | UAS-HisTag-eGFP | This study |
| ;;mZ0709-Gal4 | Mz709-gal4 | Ito et al., 1995 |
| y[1] w[*]; P{w[+mC]=UAS-mCD8::GFP.L}LL5, P{UAS-mCD8::GFP.L}2 | UASCD8GFP | BDSC_5137 |
| w[*]; P{y[+t7.7] w[+mC]=GMR56F03-GAL4}attP24/CyO | Gmr56-gal4 | BDSC_77469 |
| y[1] v[1]; P{y[+t7.7] v[+t1.8]=TRiP.JF01672}attP2 | Pink1$^{RNAi}$ | BDSC_31170 |
| w[*]; P{w[+mC]=UAS-Pink1.C}A | UAS-Pink1 | BDSC_51648 |
| w[1118]; P{y[+t7.7] w[+mC]=GMR57C10-GAL4}attP2 | nSyb-gal4 | BDSC_39171 |

| | | |
|---|---|---|
| y[1] sc[*] v[1] sev[21]; P{y[+t7.7] v[+t1.8]=TOE.GS01448}attP40 | TOE-PIG-A | BDSC_78242 |
| y[1] sc[*] v[1] sev[21]; P{y[+t7.7] v[+t1.8]=TKO.GS00769}attP40 | PIG-A $^{RNAi}$ | BDSC_76996 |
| y[1] sc[*] v[1] sev[21]; P{y[+t7.7] v[+t1.8]=TKO.GS04496}attP40 | Ccz1 $^{RNAi}$ | BDSC_82052 |
| y[1] sc[*] v[1] sev[21]; P{y[+t7.7] v[+t1.8]=TKO.GS00598}attP40/CyO | Rab7 $^{RNAi}$ | BDSC_76427 |
| y[1] v[1]; P{y[+t7.7] v[+t1.8]=TKO.GS04865}attP40 | Mon1 $^{RNAi}$ | BDSC_81817 |
| y[1] sc[*] v[1] sev[21]; P{y[+t7.7] v[+t1.8]=TRiP.HMS02460}attP40 | Vps13 $^{RNAi}$ | BDSC_38270 |
| y[1] sc[*] v[1] sev[21]; P{y[+t7.7] v[+t1.8]=TRiP.HMS05488}attP40 | CG17660$^{RNAi}$ | BDSC_67022 |
| y[1] v[1]; P{y[+t7.7] v[+t1.8]=TRiP.HMJ30013}attP40/CyO | Rhau$^{RNAi}$ | BDSC_62936 |
| y[1] v[1]; P{y[+t7.7] v[+t1.8]=TRiP.JF03249}attP2 | Proc $^{RNAi}$ | BDSC_29570 |
| y[1] sc[*] v[1] sev[21]; P{y[+t7.7] v[+t1.8]=TKO.GS05351}attP40 | CG10646$^{RNAi}$ | BDSC_85902 |
| y[1] sc[*] v[1] sev[21]; P{y[+t7.7] v[+t1.8]=TRiP.HMC05229}attP40 | fiz$^{RNAi}$ | BDSC_62222 |
| y[1] w[*]; Mi{y[+mDint2]=MIC}FASN2[MI01528] | FASN2$^{RNAi}$ | BDSC_33125 |
| y[1] w[*]; Mi{y[+mDint2]=MIC}CG10936[MI08898] | CG10936$^{RNAi}$ | BDSC_44835 |
| y[1] v[1]; P{y[+t7.7] v[+t1.8]=TRiP.JF01165}attP2 | CG15011 $^{RNAi}$ | BDSC_31589 |
| y[1] sc[*] v[1] sev[21]; P{y[+t7.7] v[+t1.8]=TRiP.HMC04857}attP40 | CG17612$^{RNAi}$ | BDSC_57540 |
| y[1] v[1]; P{y[+t7.7] v[+t1.8]=TKO.GS03320}attP40/CyO | CG2126$^{RNAi}$ | BDSC_80350 |
| y[1] v[1]; P{y[+t7.7] v[+t1.8]=TRiP.HMJ22434}attP40 | LNPK$^{RNAi}$ | BDSC_64035 |
| y[1] w[*]; Mi{y[+mDint2]=MIC}CG17712[MI03455] | CG17712$^{RNAi}$ | BDSC_37194 |
| y[1] w[*]; Mi{y[+mDint2]=MIC}pelo[MI09263] | pelo$^{RNAi}$ | BDSC_51272 |
| y[1] sc[*] v[1] sev[21]; P{y[+t7.7] v[+t1.8]=TRiP.HMS01827}attP2 | PIG-B$^{RNAi}$ | BDSC_38359 |
| y[1] sc[*] v[1] sev[21]; P{y[+t7.7] | spag$^{RNAi}$ | BDSC_38371 |

| | | |
|---|---|---|
| v[+t1.8]=TRiP.HMS01840}attP2/TM3, Sb[1] | | |
| y[1] sc[*] v[1] sev[21]; P{y[+t7.7] v[+t1.8]=TRiP.HMS00070}attP2 | Rel$^{RNAi}$ | BDSC_33661 |
| y[1] sc[*] v[1] sev[21]; P{y[+t7.7] v[+t1.8]=TOE.GS02071}attP40 | UAS-Rel | BDSC_79867 |
| y[1] sc[*] v[1] sev[21]; P{y[+t7.7] v[+t1.8]=TRiP.HMC04640}attP40 | Atac1$^{RNAi}$ | BDSC_57250 |
| y[1] sc[*] v[1] sev[21]; P{y[+t7.7] v[+t1.8]=TRiP.GLV21056}attP2 | l(3)07882$^{RNAi}$ | BDSC_35691 |
| y[1] sc[*] v[1] sev[21]; P{y[+t7.7] v[+t1.8]=TRiP.HMS00529}attP2 | Pld$^{RNAi}$ | BDSC_32839 |
| y[1] sc[*] v[1] sev[21]; P{y[+t7.7] v[+t1.8]=TRiP.HMS02243}attP2 | Rpp25$^{RNAi}$ | BDSC_41679 |
| y[1] v[1]; P{y[+t7.7] v[+t1.8]=TRiP.HMC03184}attP40 | GMF$^{RNAi}$ | BDSC_51452 |
| y[1] sc[*] v[1] sev[21]; P{y[+t7.7] v[+t1.8]=TRiP.HMS01358}attP2/TM3, Sb[1] | Atg7$^{RNAi}$ | BDSC_34369 |
| y[1] v[1]; P{y[+t7.7] v[+t1.8]=TRiP.HMJ03126}attP40 | Ada2a$^{RNAi}$ | BDSC_50905 |
| y[1] sc[*] v[1] sev[21]; P{y[+t7.7] v[+t1.8]=TRiP.HMC06224}attP2 | CG12773$^{RNAi}$ | BDSC_65949 |
| y[1] sc[*] v[1] sev[21]; P{y[+t7.7] v[+t1.8]=TRiP.HMS00328}attP2 | CG7627$^{RNAi}$ | BDSC_32337 |
| y[1] v[1]; P{y[+t7.7] v[+t1.8]=TRiP.HMS00870}attP2 | Dark$^{RNAi}$ | BDSC_33924 |
| y[1] v[1]; P{y[+t7.7] v[+t1.8]=TRiP.JF03275}attP2 | CG3703$^{RNAi}$ | BDSC_29596 |
| y[1] sc[*] v[1] sev[21]; P{y[+t7.7] v[+t1.8]=TRiP.HMS01175}attP2/TM3, Sb[1] | NiPp1$^{RNAi}$ | BDSC_34696 |
| y[1] v[1]; P{y[+t7.7] v[+t1.8]=TRiP.HMJ22813}attP40 | CG31370$^{RNAi}$ | BDSC_60456 |
| y[1] v[1]; P{y[+t7.7] v[+t1.8]=TRiP.HMJ23526}attP40 | Irbp$^{RNAi}$ | BDSC_61942 |
| y[1] v[1]; P{y[+t7.7] v[+t1.8]=TRiP.JF02313}attP2 | CG32532$^{RNAi}$ | BDSC_26750 |
| y[1] sc[*] v[1] sev[21]; P{y[+t7.7] v[+t1.8]=TRiP.HMS02243}attP2 | Rpp25$^{RNAi}$ | BDSC_41679 |
| y[1] v[1]; P{y[+t7.7] | hfw$^{RNAi}$ | BDSC_28561 |

| | | |
|---|---|---|
| v[+t1.8]=TRiP.HM05047}attP2 | | |
| y[1] v[1]; P{y[+t7.7] v[+t1.8]=TRiP.JF02192}attP2 | achi$^{RNAi}$ | BDSC_31903 |
| y[1] v[1]; P{y[+t7.7] v[+t1.8]=TRiP.HMJ23972}attP40/CyO | TTLL6A$^{RNAi}$ | BDSC_62488 |
| y[1] sc[*] v[1] sev[21]; P{y[+t7.7] v[+t1.8]=TRiP.HMC03076}attP2 | Nos$^{RNAi}$ | BDSC_50675 |
| w[1118]; P{w[+mC]=UAS-Nos.L}2 | UAS-Nos | BDSC_56823 |

**Olfactory Receptor Neurons (ORNs) axotomy**

ORN bilateral axotomy was performed on 4 ± 1 days old flies by surgical ablation of the third antennal segments. Briefly, flies were anesthetized with $CO_2$ and then both antennae were removed with Dumont #5 forceps, and returned to the vial (M. Purice, 2020; M. D. Purice et al., 2017). Flies recovered 24 hours on food at 25°C before dissection.

**Immunohistochemistry and confocal imaging – invasion phenotype**

Immunohistochemistry was performed on adult flies brains of 5 ± 1 days, with at least two independent experiments. The flies The brains were dissected in ice-cold PBS and fixed for 20 minutes in freshly prepared 3.7% paraformaldehyde (in 1x PBS, 0.3% Triton X-100 [PBX] [Sigma Aldrich]) at room temperature (RT), followed by three 15-minute washes in PBX at RT on a shaker. Then, the brains were incubated for 1 hour in blocking solution (PBX, 10% normal goat serum [NGS]) at RT. Following blocking, the brains were incubated with primary antibodies (rabbit anti-GFP [Thermo Fisher Scientific], 1:1000, mouse anti-brp [DSHB, nc82], 1:100) in blocking solution at 4°C overnight, followed by three 15-minute washes in PBX at RT. Secondary antibodies (goat anti-rabbit Alexa488, goat anti-mouse Alexa555, both at 1:1000 [Thermo Fisher Scientific]) in PBX with 10% NGS were applied overnight at 4°C. Afterward, the brains were washed three times for 15 minutes in PBT at RT on a shaker and mounted with the anterior facing up in RapiClear 1.47 (SUNJin Lab). Imaging was performed using a Nikon A1R confocal microscope with a 40x (NA 1.15) water immersion lens, Z-stacks of the entire antennal lobes were acquired. The acquisition was carried out using a Galvano scanner, with a zoom factor of 1, scan speed of 0.5, and line averaging set to 2. All images were captured with a pinhole of 0.9 Airy units and a resolution of 1024 × 1024. Z-stacks (with 0,5 µm step intervals) were obtained for data acquisition, and the same imaging settings were applied across all genotypes and sessions. Image analysis was performed using Fiji (Schindelin et al., 2009). Image analysis was performed using Fiji (Schindelin et al., 2009). Each antennal lobe is composed of

multiple glomeruli, and EG separate them and invade them when active (Doherty et al., 2009; Pogodalla et al., 2021). To quantify EG invasion in the antennal lobe, we calculated the invasion in each single glomeruli. To do so and be consistent with the section of the antennal lobe analyzed, anti-brp was used to identify the 3 Z-planes where DM6 and DM1 glomeruli were present (B. Wu et al., 2017). Then to automatically detect and segment each glomeruli of the antennal lobe section, regions of interest (ROIs) were defined in the SUM projection of the 3 Z-planes by using the Fiji plugin Stardist, which is developed to segment round objects (Weigert et al., 2019). To quantify the EG invasion in the ROIs, anti-GFP SUM projection of the same 3 Z-planes was used. The GFP intensity was detected in each ROI, and it was normalized to the area of each ROI (GFP intensity/glomeruli area) to calculate the EG invasion in each glomeruli. Then, the normalized GFP intensity of each glomeruli of an antennal lobe were summed and normalized for the number of glomeruli detected in the antennal lobe. For each experiment, the EG antennal lobe invasion of each fly was normalized to the mean of the control. Representative images show the SUM projections of the 3 Z-planes.

**Immunohistochemistry and confocal imaging – TH staining**

Immunohistochemistry was performed on adult fly brains of 22 ± 2 days, with at least two independent experiments. The brains were dissected in ice-cold PBS and fixed for 20 minutes in freshly prepared 3.7% paraformaldehyde (in 1x PBS, 0.2% Triton X-100 [PBX]) at room temperature (RT), followed by three 15-minute washes in PBX at RT on a shaker. Then, the brains were incubated for 1 hour in blocking solution (PBX, 10% normal goat serum [NGS]) at RT. Following blocking, the brains were incubated with primary antibodies (rabbit anti-TH [Sigma], 1:200, mouse anti-DLG [DSHB], 1:100) in blocking solution at 4°C for 1.5 to 2 days, followed by three 15-minute washes in PBX at RT. Secondary antibodies (goat anti-rabbit Alexa488, goat anti-mouse Alexa555, both at 1:500 [Thermo Fisher Scientific]) in PBX with 10% NGS were applied overnight at 4°C. Afterward, the brains were washed three times for 15 minutes in PBT at RT on a shaker and mounted with the anterior facing up in RapiClear 1.47 (SUNJin Lab). Imaging was performed using a Nikon A1R confocal microscope with a 20x (NA0.95) water immersion lens, Z-stacks of the entire brain were acquired. The acquisition was carried out using a Galvano scanner, with a zoom factor of 1, scan speed of 0.5, and line averaging set to 2. All images were captured with a pinhole of 2.3 Airy units and a resolution of 1024 × 1024. Z-stacks (with 3 µm step intervals) were obtained for data acquisition, and the same imaging settings were applied across all genotypes and sessions. Image analysis was performed using Fiji (Schindelin et al., 2009). To quantify dopaminergic neuron innervation of the mushroom body (MB), anti-DLG was used to identify the five z-planes containing the synaptic region of the MB lobes. The region of interest (ROI) for the MB was defined in the sum projection of the five z-planes. To exclude background signal comparable to control, the area of anti-TH fluorescence was thresholded

(using the default threshold for all z-planes) within the selected z-stacks. Quantification of the thresholded area within the ROI was performed in each z-plane, then summed and normalized to the MB ROI area for each brain individually (TH+ area/MB area). For each experiment, the individual TH+ area/MB area values were normalized to the mean of the control. Representative images show the maximum projection of five z-planes and the thresholded middle z-plane.

**Electroretinograms (EGR)**

ERGs were recorded from flies 5 ± 1 day old as previously described (Heisenberg, 1971; Slabbaert et al., 2016). Flies were immobilized on glass microscope slides using double-sided tape. For recordings, glass electrodes (borosilicate, 1.5 mm outer diameter) filled with 3 M NaCl were placed in the thorax as a reference and on the fly eye for recordings. Each fly was exposed to 5 cycles of 3 seconds of darkness, followed by a 1-second of light stimuli with LED illumination. Response to the stimuli was recorded using Axoscope 10.7 and analyzed using Clampfit 10.7 software (Molecular Devices). ERG traces were analyzed with Igor Pro 6.37 (Wave Metrics) using a custom-made macro.

**Single-cell dissociation for cell-type specific transcriptomics**

To test that EG could be isolated from the rest of the brain we used two cohorts GMR56F03> UAS-His2Av::eGFP.VK27 and nSyb-Gal4> UAS-His2Av::eGFP.VK27. To identify differentially expressed genes in EG two cohorts were used the control w1118 expressing GMR56F03> UAS-His2Av::eGFP.VK27 and *Pink1*$^{KO\text{-}WS}$ expressing GMR56F03> UAS-His2Av::eGFP.VK27. For each genotype, ten brains of flies 5 ± 1 days old were collected, with most of the laminae removed, from each experimental repeat. The dissections were performed in ice-cold PBS that contained 5 µM Actinomycin D (Sigma) to inhibit changes in gene expression during tissue processing(Y. E. Wu et al., 2017). To prevent any bias caused by different experimental batches, all the genotypes were processed in parallel. To minimize variability across batches, the same reagents and procedures were used throughout the experiment. Dissections were completed within one hour. The dissection order and the assignment of genotypes to dissectors were alternated to reduce any experimenter-related variation.

For the dissociation of brain tissue, a mix of Dispase I (0.6 mg/ml) (Sigma), Collagenase I (30 mg/ml) (Thermo Fisher), Trypsin (0.5x) (Thermo Fisher), and 5 µM Actinomycin D was used. The brains were incubated for 20 minutes at 25°C with 1000 rpm shaking, performing four triturations at 5-minute intervals. After dissociation, the cell suspension was washed with PBS containing 5 µM Actinomycin D and then filtered through a 10 µm strainer (Pluriselect), using 300 µl of PBS EDTA (Sigma) 1µM. DAPI (Invitrogen) (1:300.000) was added after filtration.

**Fluorescence Activated Cell Sorting (FACS) for cell-type specific transcriptomics**

Immediately after the dissociation, cells were sorted using a FACSAria Fusion (BD Biosciences) flow cytometer equipped with 4 lasers (405nm, 488nm, 561nm and 640nm) and a 100 µm nozzle at 20 psi. Live (DAPI-negative), GFP-positive cells were sorted into 96-well PCR plates at 300 cells per well (3 wells per genotype) using a 4-way purity mask with the FACSDiva software v9.0.1 (BD Biosciences).

**Bulk transcriptomics of EG cells**

Library preparations and sequencing for the Bulk RNA seq of the EG cells was performed using a modified Smart-seq2 protocol based on a previously published protocol (Picelli et al., 2013). Briefly, as per the protocol, 3 ul of cell lysis buffer (0.1% Triton X-100, Sigma Aldrich; 1U/ul of RNase Inhibitor, RNase OUT, Thermo Fisher; 2.5 uM Oligo dT(25), IDT; and 2.5 mM dNTP, Promega) was aliquoted in triplicate to 96 well plates (4titude, Cat. No. 4TI-0960/C). Roughly 300 cells were sorted into the wells with lysis buffer and the plate was spun down at 2000xg for 1 min prior to storage at -80*C. For the first strand synthesis, the Smart-Seq 2 plates were thawed to room temperature for a minute and subsequently spun down at 2000 xg for minute. The RNA denaturation is carried out at 72*C for 10 mins and then flash cooled on ice for 5 mins. First strand synthesis mix (1X SuperScript II first strand synthesis buffer, Thermo Fisher; 5 mM DTT, Thermo Fisher; 100 U SuperScript II reverse transcriptase enzyme, Thermo Fisher; 10 U RNAse OUT, Thermo Fisher; 1M Betaine, Sigma Aldrich; 6 mM MgCl2, Thermo Fisher; and 1 uM TSO, IDT Technologies) is added to the cell lysis mix to a total volume of 10 ul. The First strand synthesis reaction was carried out with following program: 42*C for 90 mins; 10 cycles of {50*C for 2 mins; 42*C for 2 mins}; 72*C for 15 mins; 4*C indefinite hold. PCR amplification of the first strand product was performed by adding 15 ul of the PCR mix to the first strand product (1X KAPA HiFi HotStart Ready Mix, Roche; and 0.1 uM of IS PCR primer, IDT Technologies). 22 cycles of the following PCR program was used to amplify the first strand product: 98*C for 3 mins; 22 cycles of {98*C for 20 secs; 67*C for 15 secs; 72*C for 6 mins}; 72*C for 5 mins; 4*C indefinite hold. 20 ul of Ampure XP was added to each well and mixed. Standard Ampure XP purification was carried out as per manufacturer's recommendation and the cDNA library was eluted in 17.5 ul of Elution buffer. 17 ul of the eluted library was transfered to fresh 96 well plate (4titude, Cat. No. 4TI-0960/C). 5 ul of Tn5 tagmentation mix (1X Tagment DNA buffer, Illumina; ATM mix, Illumina and cDNA library 1 ng) was prepared for cDNA fragmentation. Tn5 tagmentation was performed with following program: 55*C for 10 mins; 4*C indefinite hold. Tagementation reaction was stopped by quenching the reaction with 1.25ul of NT buffer for 5 mins (Illumina). 1.25 ul of the i5 and i7 Illumina indexes were added to the plates. Finally 3.75 ul of NPM master mix was added to the plate and mixed well and put for the index PCR amplification: 72*C for 3 mins; 95*C for 30 secs; 12

cycles of {95*C for 10 secs; 55*C for 30 secs; 72*C for 30 secs}; 72*C for 5 mins, and 4*C indefinite hold.

The indexed PCR products were pooled in a single tube and 0.8X Ampure XP purification (Beckman Coulter) was carried out as per manufacturer's recommendation and finally the sequencing library was eluted in 35.5 ul of Elution buffer (Qiagen).

SMART seq 2 libraries were sequenced on the NextSeq 500 (Illumina) sequencing platform. Sequencing was done as per the protocol recommendations: paired end read of 76 bps (read 1), 76 bps (read 2), 8 bps (index 1) and 8 bps (index 2). For a targeted sequencing depth of ~30 million reads per sample.

**Analysis of RNAseq data - Neuron vs EG**

Raw reads from neuron- vs. glia-specific FACsorting experiments were processed with the nf-core/rnaseq pipeline (Patel et al., 2020) with default parameters and the BDGP6 reference genome. The STAR-aligned and salmon-quantified expression matrix was then subset to genes known to be enriched in neurons or glia and displayed as a per gene scaled heatmap.

**Analysis of RNAseq data - EG specific differentially expressed genes**

After FACsorting of *Pink*$^{KO\text{-}ws}$ vs. control ensheathing glia, library preparation and sequencing resulting FASTQ files were cleaned with fastp (Chen et al., 2018) with default settings. Aligning and counting were carried out with STAR (Dobin et al., 2013)and the 4th 2020 FlyBase Drosophila melanogaster release (r6.35) with the –quantMode flag set as GeneCounts. For differential gene expression testing we used DESeq2 (Love et al., 2014), where we fit a negative binomial model and carried out the Wald-test. We removed experimental batch as a covariate according to the design formula ∼date+genotype. All genes below a Benjamini-Hochberg corrected p-value of 0.05 were considered deregulated.

**ScRNAseq data loading, filtering, clustering, and differential expression analysis**

Raw counts data from Pech et al., 2024, alongside cell annotations provided by the authors was loaded into Scanpy (v1.9.1) (Wolf et al., 2018) and subset to only include cells in the young control (<= 6d of age) or Pink1 samples. After subsetting the data, filtering was performed to remove any cell with less than 250 genes expressed or a percentage of counts coming from mitochondrial genes greater than 15%, data was then normalized to a total of 10,000 counts and log transformed. Highly variable genes were detected, total_counts and percent of mitochondrial reads was regressed out and finally the data was scaled to unit variance with a zero mean, clipped to a max of 10.

After data pre-processing, a PCA was performed, Harmony (Korsunsky et al., 2019) was used to correct batches using “sample_id” as a batch key, and 122 components were used for dimensionality reduction and clustering analyses. Leiden clustering was performed with a resolution of 8.0 and using the annotations from Pech et al., 2024, all cells within each cluster were labeled by taking the most common, original annotation per cluster.

Per cluster, a differential analysis was performed. First, pseudobulk counts were generated by summing the counts per cell from all cells per sample, these counts were then used in DESeq2 (v1.44.0) (Love et al., 2014) comparing Control vs Pink1 samples. The total number of genes significantly up or downregulated per cluster (padj <= 0.05 and an abs (log2foldchange) >= 1.5) was counted and plotted.

**Statistical analysis**

GraphPad Prism was used for visualization and to determine statistical significance. Datasets were tested for normal distribution using the D’Agostino-Person Omnibus and Shapiro-Wilk normality test. For normally distributed dataset ordinary one-way ANOVA was used, followed to correct for multiple comparisons by a post hoc Tukey’s test when comparing all the datasets with each other or Dunnett’s test when comparing all the datasets to a general control. For non-normally distributed datasets Kruskal-Wallis test, followed to correct for multiple comparisons by a post hoc Dunn’s test. Significance levels are defined as * is $p<0.05$, ** is $p<0.01$, *** is $p<0.001$ and ns, not significant. ‘N’ in the legends is used to indicate how many animals were analyzed. Data are plotted as mean ± SD. Specifics on the statistical test used for each analysis are reported in the figure legends.

**Acknowledgments**

We thank the Vlaams Supercomputer Centrum, the VIB Nucleomics Cores, and the Bloomington Drosophila Stock Center (NIH P40OD018537). We are grateful to the members of the Verstreken lab for valuable discussions. R.P. was supported by PhD/postdoc fellowships from EMBO long-term fellowship. Research support was provided in part by the Leuven University Fund and Opening the Future, ERC, the Chan Zuckerberg Initiative, a Methusalem grant from the Flemish government, and FWO Vlaanderen. P.V. is an alumnus of the FENS-Kavli Network of Excellence.

Cartoons/models/illustrations were created in https://BioRender.com

**Author contributions**

Conceptualization, L.G., R.P., P.V.;

Methodology, L.G., U.P., N.S., J.L., K.D., R.P., P.V.;

Software, L.G., K.D., R.P.;

Validation, L.G., K.D., R.P.;

Formal analysis, L.G., K.D., R.P.;

Investigation, L.G., U.P., N.S., J.L., K.D., R.P.;

Writing -Original Draft, L.G., R.P., P.V.;

Writing – review and editing, all co-authors read and edited the manuscript.

Visualization, L.G., K.D., R.P.;

Supervision, R.P., P.V.;

Project administration, L.G.;

Funding acquisition, R.P., P.V.;

**Bibliography**

Agarwal, D., Sandor, C., Volpato, V., Caffrey, T. M., Monzón-Sandoval, J., Bowden, R., Alegre-Abarrategui, J., Wade-Martins, R., & Webber, C. (2020). A single-cell atlas of the human substantia nigra reveals cell-specific pathways associated with neurological disorders. *Nature Communications*, *11*(1), 1–11. https://doi.org/10.1038/s41467-020-17876-0

Bischof, J., Maeda, R. K., Hediger, M., Karch, F., & Basler, K. (2007). An optimized transgenesis system for Drosophila using germ-line-specific ϕC31 integrases. *Proceedings of the National Academy of Sciences of the United States of America*, *104*(9), 3312–3317. https://doi.org/10.1073/pnas.0611511104

Borchers, A.-C., Janz, M., Schäfer, J.-H., Moeller, A., Kümmel, D., Paululat, A., Ungermann, C., & Langemeyer, L. (2023). Regulatory sites in the Mon1–Ccz1 complex control Rab5 to Rab7 transition and endosome maturation. *Proceedings of the National Academy of Sciences*, *120*(30). https://doi.org/10.1073/pnas.2303750120

Bryois, J., Skene, N. G., Hansen, T. F., Kogelman, L. J. A., Watson, H. J., Liu, Z., Adan, R., Alfredsson, L., Ando, T., Andreassen, O., Baker, J., Bergen, A., Berrettini, W., Birgegård, A., Boden, J., Boehm, I.,

Boni, C., Boraska Perica, V., Brandt, H., … Sullivan, P. F. (2020). Genetic identification of cell types underlying brain complex traits yields insights into the etiology of Parkinson's disease. *Nature Genetics*, *52*(5), 482–493. https://doi.org/10.1038/s41588-020-0610-9

Chen, S., Zhou, Y., Chen, Y., & Gu, J. (2018). Fastp: An ultra-fast all-in-one FASTQ preprocessor. *Bioinformatics*, *34*(17), i884–i890. https://doi.org/10.1093/bioinformatics/bty560

Delgado, M. G., Oliva, C., López, E., Ibacache, A., Galaz, A., Delgado, R., Barros, L. F., & Sierralta, J. (2018). Chaski, a novel Drosophila lactate/pyruvate transporter required in glia cells for survival under nutritional stress. *Scientific Reports*, *8*(1), 1–13. https://doi.org/10.1038/s41598-018-19595-5

Dobin, A., Davis, C. A., Schlesinger, F., Drenkow, J., Zaleski, C., Jha, S., Batut, P., Chaisson, M., & Gingeras, T. R. (2013). STAR: Ultrafast universal RNA-seq aligner. *Bioinformatics*, *29*(1), 15–21. https://doi.org/10.1093/bioinformatics/bts635

Doherty, J., Logan, M. A., Taşdemir, Ö. E., & Freeman, M. R. (2009). Ensheathing Glia Function as Phagocytes in the Adult Drosophila Brain. *The Journal of Neuroscience*, *29*(15), 4768–4781. https://doi.org/10.1523/JNEUROSCI.5951-08.2009

Epp, N., Rethmeier, R., Krämer, L., & Ungermann, C. (2011). Membrane dynamics and fusion at late endosomes and vacuoles - Rab regulation, multisubunit tethering complexes and SNAREs. *European Journal of Cell Biology*, *90*(9), 779–785. https://doi.org/10.1016/j.ejcb.2011.04.007

Ettle, B., Schlachetzki, J. C. M., & Winkler, J. (2016). Oligodendroglia and Myelin in Neurodegenerative Diseases: More Than Just Bystanders? *Molecular Neurobiology*, *53*(5), 3046–3062. https://doi.org/10.1007/s12035-015-9205-3

Freeman, M. R., & Doherty, J. (2006). Glial cell biology in Drosophila and vertebrates. In *Trends in Neurosciences* (Vol. 29, Issue 2, pp. 82–90). Elsevier Current Trends. https://doi.org/10.1016/j.tins.2005.12.002

Gaudet, P., Livstone, M. S., Lewis, S. E., & Thomas, P. D. (2011). Phylogenetic-based propagation of functional annotations within the Gene Ontology consortium. *Briefings in Bioinformatics*, *12*(5), 449–462. https://doi.org/10.1093/bib/bbr042

Gershlick, D. C., Schindler, C., Chen, Y., & Bonifacino, J. S. (2016). TSSC1 is novel component of the endosomal retrieval machinery. *Molecular Biology of the Cell*, *27*(18), 2867–2878. https://doi.org/10.1091/mbc.e16-04-0209

Grossmann, D., Malburg, N., Glaß, H., Weeren, V., Sondermann, V., Pfeiffer, J. F., Petters, J., Lukas, J.,

Seibler, P., Klein, C., Grünewald, A., & Hermann, A. (2023). Mitochondria–Endoplasmic Reticulum Contact Sites Dynamics and Calcium Homeostasis Are Differentially Disrupted in PINK1-PD or PRKN-PD Neurons. *Movement Disorders*, *38*(10), 1822–1836. https://doi.org/10.1002/mds.29525

Hardie, R. C., & Raghu, P. (2001). Visual transduction in Drosophila. *Nature*, *413*(6852), 186–193.

Heisenberg, M. (1971). Separation of receptor and lamina potentials in the electroretinogram of normal and mutant Drosophila. *Journal of Experimental Biology*, *55*(1), 85–100. https://doi.org/10.1242/jeb.55.1.85

Ito, K., Urban, J., & Technau, G. M. (1995). Distribution, classification, and development ofDrosophila glial cells in the late embryonic and early larval ventral nerve cord. *Roux's Archives of Developmental Biology*, *204*(5), 284–307. https://doi.org/10.1007/BF02179499

Kaempf, N., Valadas, J. S., Robberechts, P., Schoovaerts, N., Praschberger, R., Ortega, A., Kilic, A., Chabot, D., Pech, U., Kuenen, S., Vilain, S., Baz, E.-S., Singh, J., Davis, J., Liu, S., & Verstreken, P. (2024). Behavioral screening defines three molecular Parkinsonism subgroups in Drosophila. In *bioRxiv*. https://doi.org/10.1101/2024.08.27.609924

Kane, L. A., Lazarou, M., Fogel, A. I., Li, Y., Yamano, K., Sarraf, S. A., Banerjee, S., & Youle, R. J. (2014). PINK1 phosphorylates ubiquitin to activate Parkin E3 ubiquitin ligase activity. *Journal of Cell Biology*, *205*(2), 143–153. https://doi.org/10.1083/jcb.201402104

Korsunsky, I., Millard, N., Fan, J., Slowikowski, K., Zhang, F., Wei, K., Baglaenko, Y., Brenner, M., Loh, P. ru, & Raychaudhuri, S. (2019). Fast, sensitive and accurate integration of single-cell data with Harmony. *Nature Methods*, *16*(12), 1289–1296. https://doi.org/10.1038/s41592-019-0619-0

Kremer, M. C., Jung, C., Batelli, S., Rubin, G. M., & Gaul, U. (2017). The glia of the adult Drosophila nervous system. *Glia*, *65*(4), 606–638. https://doi.org/10.1002/glia.23115

Kumar, N., Leonzino, M., Hancock-Cerutti, W., Horenkamp, F. A., Li, P., Lees, J. A., Wheeler, H., Reinisch, K. M., & De Camilli, P. (2018). VPS13A and VPS13C are lipid transport proteins differentially localized at ER contact sites. *Journal of Cell Biology*, *217*(10), 3625–3639. https://doi.org/10.1083/jcb.201807019

Lang, A. E., & Lozano, A. M. (1998). Parkinson's Disease. *New England Journal of Medicine*, *339*(15), 1044–1053. https://doi.org/10.1056/NEJM199810083391506

Lappe-Siefke, C., Goebbels, S., Gravel, M., Nicksch, E., Lee, J., Braun, P. E., Griffiths, I. R., & Nave, K.-A. (2003). Disruption of Cnp1 uncouples oligodendroglial functions in axonal support and

myelination. *Nature Genetics*, *33*(3), 366–374. https://doi.org/10.1038/ng1095

Lesage, S., Drouet, V., Majounie, E., Deramecourt, V., Jacoupy, M., Nicolas, A., Cormier-Dequaire, F., Hassoun, S. M., Pujol, C., Ciura, S., Erpapazoglou, Z., Usenko, T., Maurage, C., Sahbatou, M., Liebau, S., Ding, J., Bilgic, B., Emre, M., Erginel-Unaltuna, N., … Brice, A. (2016). Loss of VPS13C Function in Autosomal-Recessive Parkinsonism Causes Mitochondrial Dysfunction and Increases PINK1/Parkin-Dependent Mitophagy. *The American Journal of Human Genetics*, *98*(3), 500–513. https://doi.org/10.1016/j.ajhg.2016.01.014

Love, M. I., Huber, W., & Anders, S. (2014). Moderated estimation of fold change and dispersion for RNA-seq data with DESeq2. *Genome Biology*, *15*(12), 1–21. https://doi.org/10.1186/s13059-014-0550-8

MacDonald, J. M., Beach, M. G., Porpiglia, E., Sheehan, A. E., Watts, R. J., & Freeman, M. R. (2006). The Drosophila Cell Corpse Engulfment Receptor Draper Mediates Glial Clearance of Severed Axons. *Neuron*, *50*(6), 869–881. https://doi.org/10.1016/j.neuron.2006.04.028

Morais, V. A., Haddad, D., Craessaerts, K., De Bock, P.-J., Swerts, J., Vilain, S., Aerts, L., Overbergh, L., Grünewald, A., Seibler, P., Klein, C., Gevaert, K., Verstreken, P., & De Strooper, B. (2014). PINK1 Loss-of-Function Mutations Affect Mitochondrial Complex I Activity via NdufA10 Ubiquinone Uncoupling. *Science*, *344*(6180), 203–207. https://doi.org/10.1126/science.1249161

Morais, V. A., Verstreken, P., Roethig, A., Smet, J., Snellinx, A., Vanbrabant, M., Haddad, D., Frezza, C., Mandemakers, W., Vogt-Weisenhorn, D., Van Coster, R., Wurst, W., Scorrano, L., & De Strooper, B. (2009). Parkinson's disease mutations in PINK1 result in decreased Complex I activity and deficient synaptic function. *EMBO Molecular Medicine*, *1*(2), 99–111. https://doi.org/10.1002/emmm.200900006

Munhoz, R. P., Moro, A., Silveira-moriyama, L., & Teive, H. A. (2015). Non-motor signs in Parkinson ' s disease : a review. *Arq. Neuropsiquiatr.*, *January*, 454–462. https://doi.org/10.1590/0004-282X20150029

Muñoz-Braceras, S., Tornero-Écija, A. R., Vincent, O., & Escalante, R. (2019). VPS13A, a closely associated mitochondrial protein, is required for efficient lysosomal degradation. *Disease Models & Mechanisms*, *12*(2). https://doi.org/10.1242/dmm.036681

Narendra, D. P., Jin, S. M., Tanaka, A., Suen, D.-F., Gautier, C. A., Shen, J., Cookson, M. R., & Youle, R. J. (2010). PINK1 Is Selectively Stabilized on Impaired Mitochondria to Activate Parkin. *PLoS Biology*, *8*(1), e1000298. https://doi.org/10.1371/journal.pbio.1000298

Narendra, D. P., & Youle, R. J. (2024). The role of PINK1–Parkin in mitochondrial quality control. *Nature Cell Biology*, *26*(10), 1639–1651. https://doi.org/10.1038/s41556-024-01513-9

Otto, N., Marelja, Z., Schoofs, A., Kranenburg, H., Bittern, J., Yildirim, K., Berh, D., Bethke, M., Thomas, S., Rode, S., Risse, B., Jiang, X., Pankratz, M., Leimkühler, S., & Klämbt, C. (2018). The sulfite oxidase Shopper controls neuronal activity by regulating glutamate homeostasis in Drosophila ensheathing glia. *Nature Communications*, *9*(1), 3514. https://doi.org/10.1038/s41467-018-05645-z

Patel, H., Ewels, P., Manning, J., Garcia, M. U., Peltzer, A., Hammarén, R., Botvinnik, O., Talbot, A., Sturm, G., Bot, N., Zepper, M., Moreno, D., Vemuri, P., Binzer-Panchal, M., Greenberg, E., Silviamorins, Pantano, L., Syme, R., Kelly, G., … Gabernet, G. (2020). nf-core/rnaseq: nf-core/rnaseq. In *Zenodo*. https://doi.org/10.5281/zenodo.1400710.

Pech, U., Janssens, J., Schoovaerts, N., Kuenen, S., Makhzami, S., Hulselmans, G., Poovathingal, S., Bademosi, A. T., Swerts, J., Vilain, S., Aerts, S., & Verstreken, P. (2024). *Synaptic deregulation of cholinergic projection neurons causes olfactory dysfunction across 5 fly Parkinsonism models*. 1–35. https://doi.org/10.7554/eLife.98348.1

Picelli, S., Björklund, Å. K., Faridani, O. R., Sagasser, S., Winberg, G., & Sandberg, R. (2013). Smart-seq2 for sensitive full-length transcriptome profiling in single cells. *Nature Methods*, *10*(11), 1096–1100. https://doi.org/10.1038/nmeth.2639

Pogodalla, N., Kranenburg, H., Rey, S., Rodrigues, S., Cardona, A., & Klämbt, C. (2021). Drosophila ßHeavy-Spectrin is required in polarized ensheathing glia that form a diffusion-barrier around the neuropil. *Nature Communications*, *12*(1), 6357. https://doi.org/10.1038/s41467-021-26462-x

Pogson, J. H., Ivatt, R. M., Sanchez-Martinez, A., Tufi, R., Wilson, E., Mortiboys, H., & Whitworth, A. J. (2014). The Complex I Subunit NDUFA10 Selectively Rescues Drosophila pink1 Mutants through a Mechanism Independent of Mitophagy. *PLoS Genetics*, *10*(11), e1004815. https://doi.org/10.1371/journal.pgen.1004815

Praschberger, R., Kuenen, S., Schoovaerts, N., Kaempf, N., Singh, J., Janssens, J., Swerts, J., Nachman, E., Calatayud, C., Aerts, S., Poovathingal, S., & Verstreken, P. (2023). Neuronal identity defines α-synuclein and tau toxicity. *Neuron*, *111*(10), 1577-1590.e11. https://doi.org/10.1016/j.neuron.2023.02.033

Purice, M. (2020). Olfactory receptor neuron (ORN) axotomy assay. *Bio-Protocol Preprint*.

https://doi.org/bio-protocol.org/prep625

Purice, M. D., Ray, A., Münzel, E. J., Pope, B. J., Park, D. J., Speese, S. D., & Logan, M. A. (2017). A novel Drosophila injury model reveals severed axons are cleared through a draper/MMP-1 signaling cascade. *ELife*, *6*, 1–30. https://doi.org/10.7554/eLife.23611

Saab, A. S., Tzvetavona, I. D., Trevisiol, A., Baltan, S., Dibaj, P., Kusch, K., Möbius, W., Goetze, B., Jahn, H. M., Huang, W., Steffens, H., Schomburg, E. D., Pérez-Samartín, A., Pérez-Cerdá, F., Bakhtiari, D., Matute, C., Löwel, S., Griesinger, C., Hirrlinger, J., … Nave, K. A. (2016). Oligodendroglial NMDA Receptors Regulate Glucose Import and Axonal Energy Metabolism. *Neuron*, *91*(1), 119–132. https://doi.org/10.1016/j.neuron.2016.05.016

Schindelin, J., Arganda-Carrera, I., Frise, E., Verena, K., Mark, L., Tobias, P., Stephan, P., Curtis, R., Stephan, S., Benjamin, S., Jean-Yves, T., Daniel, J. W., Volker, H., Kevin, E., Pavel, T., & Albert, C. (2009). Fiji - an Open platform for biological image analysis. *Nature Methods*, *9*(7). https://doi.org/10.1038/nmeth.2019.Fiji

Slabbaert, J. R., Kuenen, S., Swerts, J., Maes, I., Uytterhoeven, V., Kasprowicz, J., Fernandes, A. C., Blust, R., & Verstreken, P. (2016). Shawn, the Drosophila homolog of SLC25A39/40, is a mitochondrial carrier that promotes neuronal survival. *Journal of Neuroscience*, *36*(6), 1914–1929. https://doi.org/10.1523/JNEUROSCI.3432-15.2016

Smajic, S., Prada-Medina, C. A., Landoulsi, Z., Ghelfi, J., Delcambre, S., Dietrich, C., Jarazo, J., Henck, J., Balachandran, S., Pachchek, S., Morris, C. M., Antony, P., Timmermann, B., Sauer, S., Pereira, S. L., Schwamborn, J. C., May, P., Grunewald, A., & Spielmann, M. (2022). Single-cell sequencing of human midbrain reveals glial activation and a Parkinson-specific neuronal state. *Brain*, *145*(3), 964–978. https://doi.org/10.1093/brain/awab446

Soukup, S., Kuenen, S., Vanhauwaert, R., Geens, A., Strooper, B. De, & Verstreken, P. (2016). *A LRRK2-Dependent EndophilinA Phosphoswitch Is Critical for Macroautophagy at Presynaptic Article A LRRK2-Dependent EndophilinA Phosphoswitch Is Critical for Macroautophagy at Presynaptic Terminals*. 829–844. https://doi.org/10.1016/j.neuron.2016.09.037

Suárez-Pozos, E., Thomason, E. J., & Fuss, B. (2020). Glutamate Transporters: Expression and Function in Oligodendrocytes. *Neurochemical Research*, *45*(3), 551–560. https://doi.org/10.1007/s11064-018-02708-x

Valadas, J. S., Esposito, G., Vandekerkhove, D., Miskiewicz, K., Deaulmerie, L., Raitano, S., Seibler, P., Klein, C., & Verstreken, P. (2018). ER Lipid Defects in Neuropeptidergic Neurons Impair Sleep

Patterns in Parkinson's Disease. *Neuron*, *98*(6), 1155-1169.e6. https://doi.org/10.1016/j.neuron.2018.05.022

Vonk, J. J., Yeshaw, W. M., Pinto, F., Faber, A. I. E., Lahaye, L. L., Kanon, B., van der Zwaag, M., Velayos-Baeza, A., Freire, R., van IJzendoorn, S. C., Grzeschik, N. A., & Sibon, O. C. M. (2017). Drosophila Vps13 Is Required for Protein Homeostasis in the Brain. *PLOS ONE*, *12*(1), e0170106. https://doi.org/10.1371/journal.pone.0170106

Vrijsen, S., Vrancx, C., Del Vecchio, M., Swinnen, J. V., Agostinis, P., Winderickx, J., Vangheluwe, P., & Annaert, W. (2022). Inter-organellar Communication in Parkinson's and Alzheimer's Disease: Looking Beyond Endoplasmic Reticulum-Mitochondria Contact Sites. *Frontiers in Neuroscience*, *16*. https://doi.org/10.3389/fnins.2022.900338

Weigert, M., Schmidt, U., Haase, R., Sugawara, K., & Myers, G. (2019). *Star-convex Polyhedra for 3D Object Detection and Segmentation in Microscopy*. http://arxiv.org/abs/1908.03636

Wolf, F. A., Angerer, P., & Theis, F. J. (2018). SCANPY: large-scale single-cell gene expression data analysis. *Genome Biology*, *19*(1), 15. https://doi.org/10.1186/s13059-017-1382-0

Wong, Y. C., Peng, W., & Krainc, D. (2019). Lysosomal Regulation of Inter-mitochondrial Contact Fate and Motility in Charcot-Marie-Tooth Type 2. *Developmental Cell*, *50*(3), 339-354.e4. https://doi.org/10.1016/j.devcel.2019.05.033

Wong, Y. C., Ysselstein, D., & Krainc, D. (2018). Mitochondria–lysosome contacts regulate mitochondrial fission via RAB7 GTP hydrolysis. *Nature*, *554*(7692), 382–386. https://doi.org/10.1038/nature25486

Wu, B., Li, J., Chou, Y.-H., Luginbuhl, D., & Luo, L. (2017). Fibroblast growth factor signaling instructs ensheathing glia wrapping of Drosophila olfactory glomeruli. *Proceedings of the National Academy of Sciences*, *114*(29), 7505–7512. https://doi.org/10.1073/PNAS.1706533114

Wu, C. F., & Wong, F. (1977). Frequency characteristics in the visual system of Drosophila: Genetic dissection of electroretinogram components. *Journal of General Physiology*, *69*(6), 705–724. https://doi.org/10.1085/jgp.69.6.705

Wu, Y. E., Pan, L., Zuo, Y., Li, X., & Hong, W. (2017). Detecting Activated Cell Populations Using Single-Cell RNA-Seq. *Neuron*, *96*(2), 313-329.e6. https://doi.org/10.1016/j.neuron.2017.09.026

Yamano, K., Wang, C., Sarraf, S. A., Münch, C., Kikuchi, R., Noda, N. N., Hizukuri, Y., Kanemaki, M. T., Harper, W., Tanaka, K., Matsuda, N., & Youle, R. J. (2018). Endosomal Rab cycles regulate Parkin-mediated mitophagy. *ELife*, *7*, 1–32. https://doi.org/10.7554/eLife.31326

Yildirim, K., Petri, J., Kottmeier, R., & Klämbt, C. (2019). Drosophila glia: Few cell types and many conserved functions. *Glia*, *67*(1), 5–26. https://doi.org/10.1002/glia.23459

**Figure 1**

(**A**) tSNE of the cells of *Pink1*$^{P399L}$ knock-in mutants (5 days old). Cell types are labeled with colors indicating the number of deregulated genes compared to control. EG are encircled and labeled. (**B-B"**) (**B**) SUM intensity of confocal images of fly brains (5 ± 1 days old) stained with anti-GFP (Green) and anti-Brp (Magenta), where anti-GFP marks EG and anti-Brp marks presynaptic sites of the antennal lobes. Scale bar: 20 µm (**B'**) SUM intensity of confocal images of control flies vs control flies 24 hours after ORNs severing. (**B"**) SUM intensity of confocal images of *Pink1*$^{KO-WS}$ vs *Pink1*$^{KO-WS}$ flies 24 hours after ORNs severing. (**C**) Quantification of GFP intensity with the glomeruli of the antennal lobe area in 5 ± 1 days old flies (as in B) relative to the control. ANOVA with Dunnet's multiple comparison test, * is p<0.05, ** is p<0.01, *** is p<0.001. Bars: mean ± SD; points are individual animals N≥13 per genotype. (**D-D"**) SUM intensity of confocal images of fly brains (5 ± 1 days old) stained with anti-GFP (Green) and anti-Brp (Magenta), where anti-GFP marks EG and anti-Brp marks presynaptic sites of the antennal lobes. Scale bar: 20 µm. (**D'**) SUM intensity of confocal images of *w1118* with *Pink1* downregulation in EG. (**D"**) SUM intensity of confocal images of *Pink1*$^{KO-WS}$ with *Pink1* rescued in EG. (**E**) Quantification of GFP intensity within the glomeruli of the antennal lobe area in 5 days old flies (as in D) relative to the control. ANOVA with Tukey's multiple comparison test, * is p<0.05, ** is p<0.01, *** is p<0.001. Bars: mean ± SD; points are individual animals N≥10 per genotype.

**Figure 2**

(**A**) Representative ERG traces: ON peak is highlighted by the arrow. (**B**) Normalized ON peak response of flies (5 ± 1 days old). ANOVA with Tukey's multiple comparison test, * is p<0.05, ** is p<0.01, *** is p<0.001. Bars: mean ± SD; points are individual animals N≥11 per genotype. (**C-C"**) (**C**) Maximum projection confocal image of control and *Pink1*$^{KO-WS}$ in Mushroom Bodies (MB) of aged flies (22 ± 2 days old), stained with anti-TH (cyan) and anti-DLG (magenta) antibodies, DLG is used to mark post-synaptic site of MB. The black and white image is the middle Z-plan within the region of interest of the MB(ROI, yellow), it is used to represent the thresholded TH area (white). Scale bar: 20 µm. (**C'**) Maximum projection confocal image of *w1118* with *Pink1* downregulation in EG. (**C"**) Maximum projection confocal image of *Pink1*$^{KO-WS}$ with *Pink1* rescued in EG. (**D**) Quantification of dopaminergic synaptic area within MB in aged flies (22 ± 2 days old). ANOVA with Tukey's multiple comparison test, * is p<0.05, ** is p<0.01, *** is p<0.001. Bars: mean ± SD; points are individual animals N≥12 per genotype.

**Figure 3**

(**A**) Scheme of cell-type specific transcriptomics. (**B**) Scaled gene expression of representative genes for EG and neurons after sorting EG or neurons using the protocol described in figure A. Figure generated using R studio (R Core Team, 2022). (**C**) Differentially expressed genes in EG in *Pink1*$^{KO\text{-}WS}$ compared to control flies, plotted according to their Log2 Fold change and the -Log10 of the adjusted p-value. Intercept in RED (-Log10 adjusted p-value = 4.31). *Two data points are outside the boundaries of the plot. (**D**) ERG ON peak value differences to *Pink1*$^{KO\text{-}WS}$ (red) flies (5 ± 1 days old) of *Pink1*$^{KO\text{-}WS}$ flies (5 ± 1 days old) with DEGs downregulated, or upregulated, specifically in EG. ON peak value are expressed as the difference to *Pink1*$^{KO\text{-}WS}$. ANOVA with Dunnett's test, * is $p<0.05$, ** is $p<0.01$, *** is $p<0.001$. Bars: mean ± SD; points are individual animals N≥3 per genotype. *One data point is outside the boundaries of the plot.

**Figure 4**

(**A-A'**) (**A**) Representative ERG traces. (**A'**) Representative ERG traces of genes *Pink1*$^{KO\text{-}WS}$ flies with *Vps13, mon1,* and *rab7* downregulated in EG (**B**) Normalized ON peak response of flies (5 ± 1 days old). Kruskal-Wallis with Dunn's multiple comparison test, * is $p<0.05$, ** is $p<0.01$, *** is $p<0.001$. Bars: mean ± SD; points are individual animals N≥8 per genotype. (**C**) Maximum projection confocal image of control and *Pink1*$^{KO\text{-}WS}$ in Mushroom Bodies (MB) of aged flies (22 ± 2 days old), stained with anti-TH (cyan) and anti-DLG (magenta) antibodies, DLG is used to mark post-synaptic site of MB. The black and white image is the middle Z-plan within the region of interest of the MB(ROI, yellow), it is used to represent the thresholded TH area (white). Scale bar: 20 µm. (**D**) Quantification of dopaminergic synaptic area within MB in aged flies (22 ± 2 days old). ANOVA with Dunnett's multiple comparison test, * is $p<0.05$, ** is $p<0.01$, *** is $p<0.001$. Bars: mean ± SD; points are individual animals N≥13 per genotype.

**Declaration of interests**

P.V. is the scientific founder of Jay Therapeutics. All other authors declare no competing interests.

**Inclusion and diversity**

We support inclusive, diverse, and equitable conduct of research.

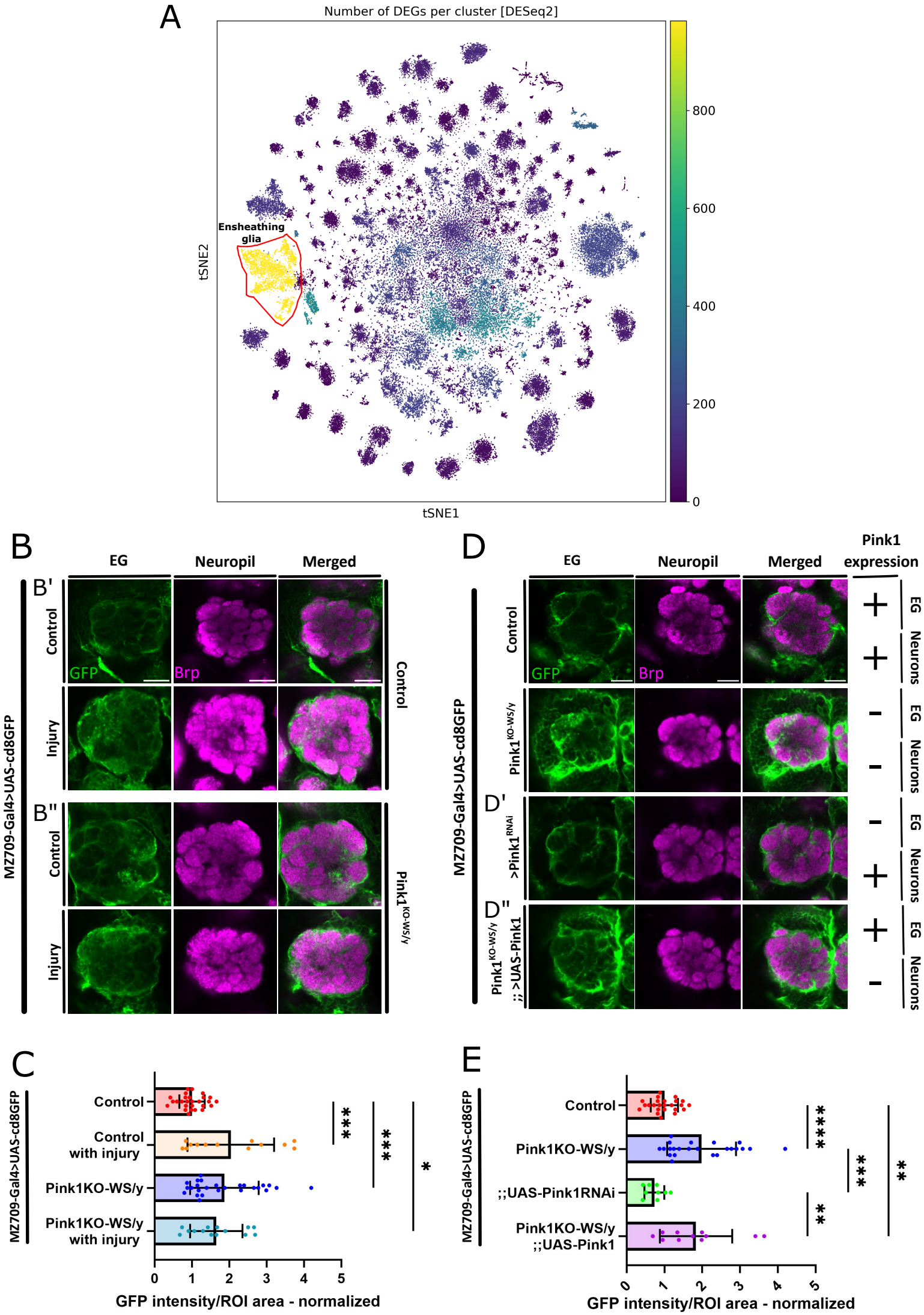
A
Number of DEGs per cluster [DESeq2]
Ensheathing glia
tSNE2
tSNE1
800
600
400
200
0
B
EG
Neuropil
Merged
B'
B''
Control
Injury
GFP
Brp
MZ709-Gal4>UAS-cd8GFP
Pink1KO-WS/y
D
Pink1 expression
D'
D''
>Pink1RNAi
;; >UAS-Pink1
EG
Neurons
C
Control
Control with injury
Pink1KO-WS/y
Pink1KO-WS/y with injury
GFP intensity/ROI area - normalized
E
;;UAS-Pink1RNAi
Pink1KO-WS/y ;;UAS-Pink1

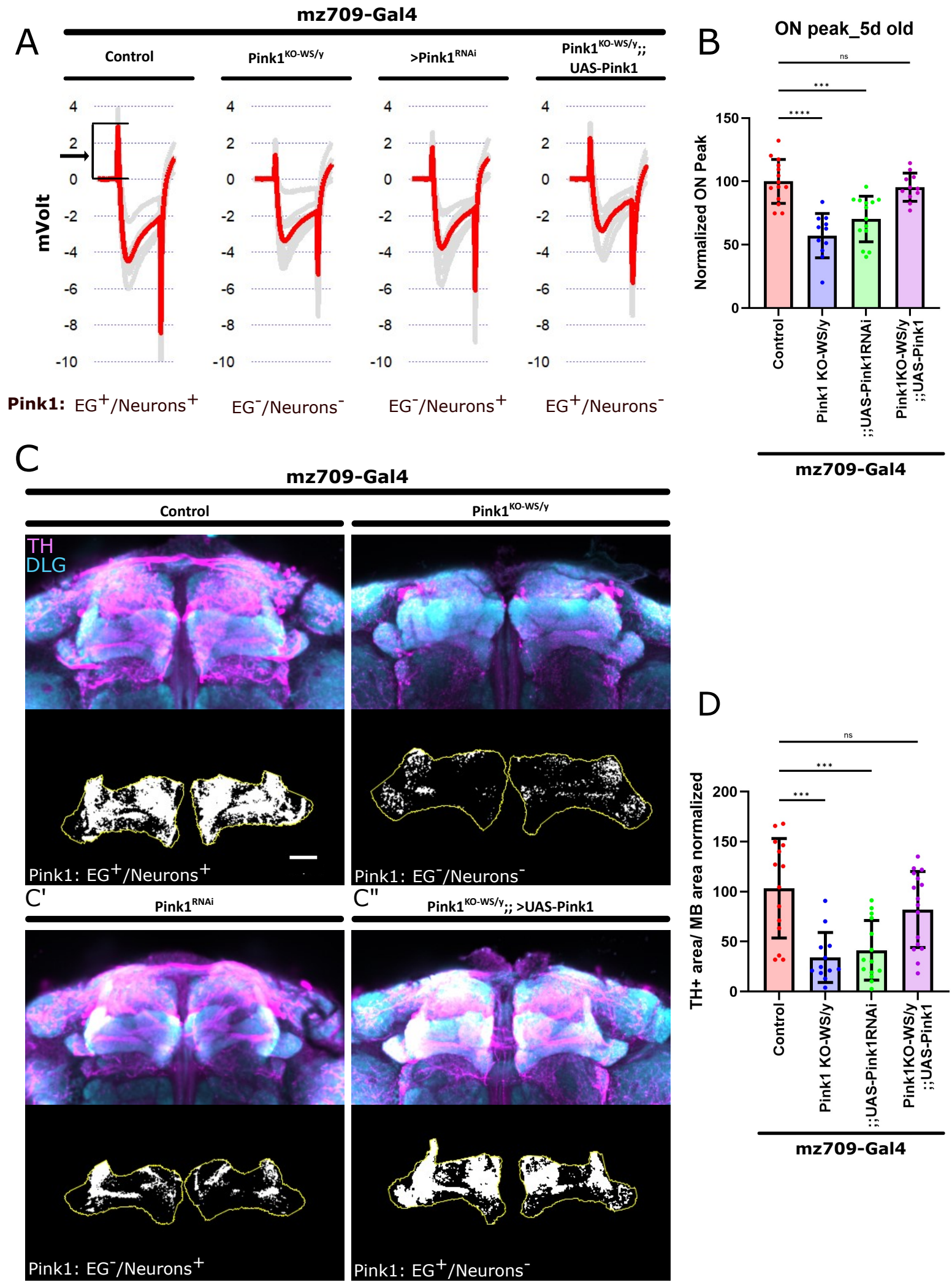
A
mz709-Gal4
Control
Pink1KO-WS/y
>Pink1RNAi
Pink1KO-WS/y;; UAS-Pink1
mVolt
4
2
0
-2
-4
-6
-8
-10
Pink1: EG+/Neurons+
EG-/Neurons-
EG-/Neurons+
EG+/Neurons-
B
ON peak_5d old
ns
***
****
Normalized ON Peak
150
100
50
0
Control
Pink1 KO-WS/y
;;UAS-Pink1RNAi
Pink1KO-WS/y ;;UAS-Pink1
mz709-Gal4
C
mz709-Gal4
Control
Pink1KO-WS/y
TH
DLG
Pink1: EG+/Neurons+
Pink1: EG-/Neurons-
C'
Pink1RNAi
C''
Pink1KO-WS/y;; >UAS-Pink1
Pink1: EG-/Neurons+
Pink1: EG+/Neurons-
D
ns
***
***
TH+ area/ MB area normalized
200
150
100
50
0
Control
Pink1 KO-WS/y
;;UAS-Pink1RNAi
Pink1KO-WS/y ;;UAS-Pink1
mz709-Gal4

A

CELL-TYPE SPECIFIC TRANSCRIPTOMIC

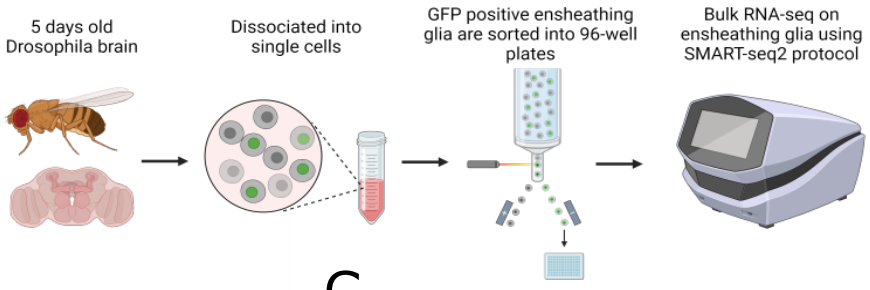


B

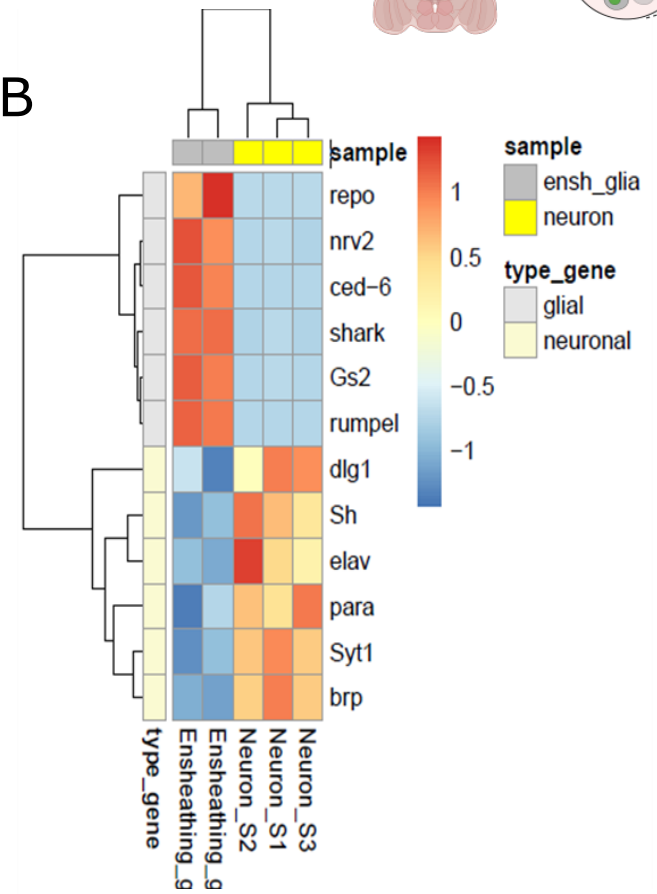


C

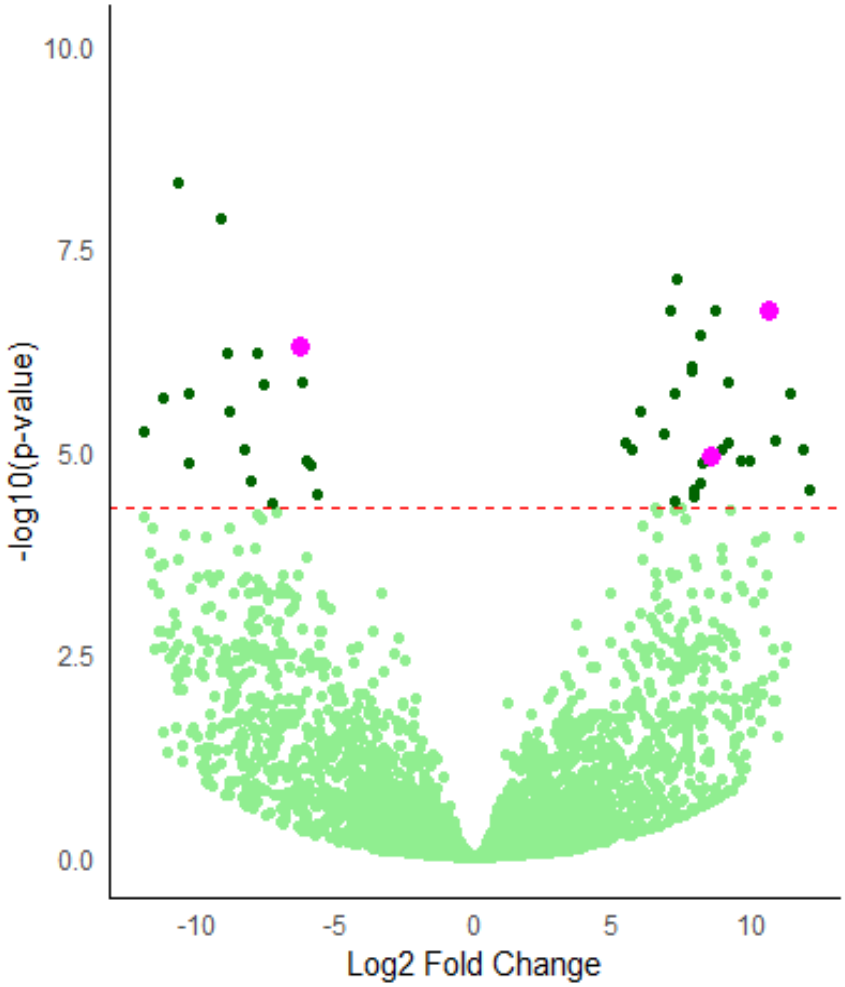


D

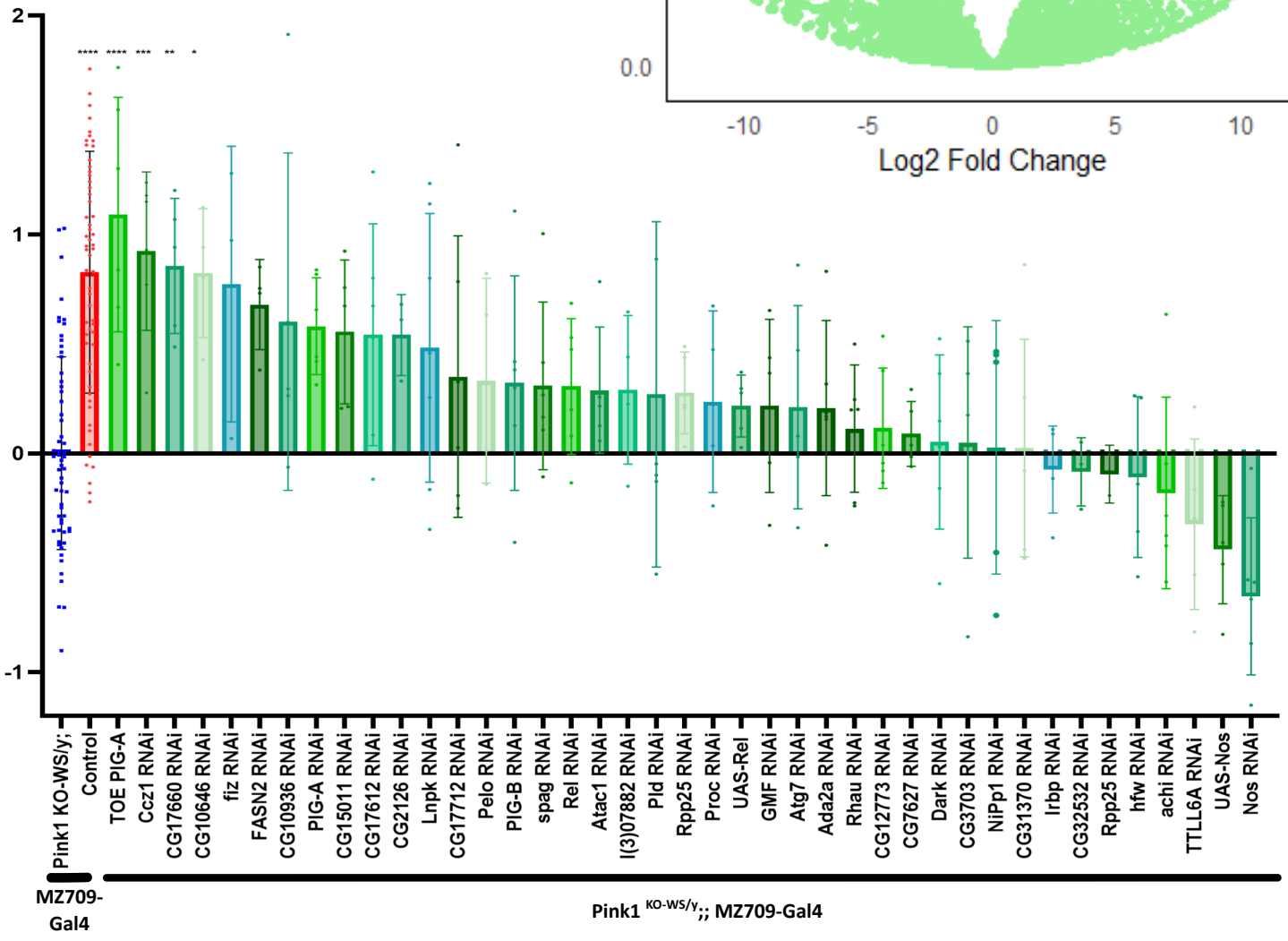

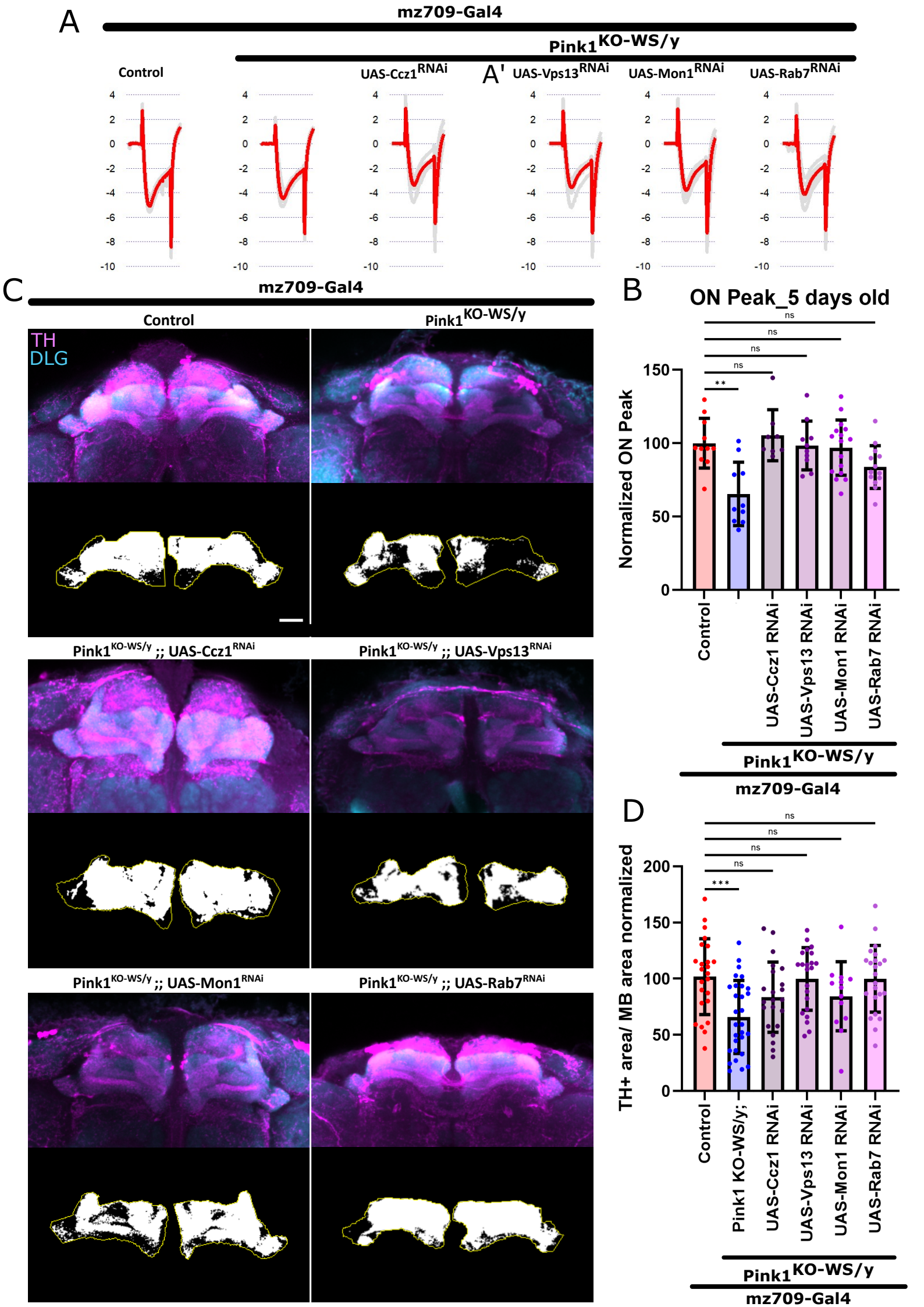
A
mz709-Gal4
Pink1KO-WS/y
Control
UAS-Ccz1RNAi
A'
UAS-Vps13RNAi
UAS-Mon1RNAi
UAS-Rab7RNAi
C
mz709-Gal4
Control
Pink1KO-WS/y
TH
DLG
Pink1KO-WS/y ;; UAS-Ccz1RNAi
Pink1KO-WS/y ;; UAS-Vps13RNAi
Pink1KO-WS/y ;; UAS-Mon1RNAi
Pink1KO-WS/y ;; UAS-Rab7RNAi
B
ON Peak_5 days old
Normalized ON Peak
ns
**
Control
UAS-Ccz1 RNAi
UAS-Vps13 RNAi
UAS-Mon1 RNAi
UAS-Rab7 RNAi
Pink1KO-WS/y
mz709-Gal4
D
TH+ area/ MB area normalized
***
Pink1 KO-WS/y;
Pink1KO-WS/y
mz709-Gal4